

# Manganese Based Perovskites in Ethanol Steam Reforming

G. Perin<sup>1</sup> · M. Guiotto<sup>2</sup> · M. M. Natile<sup>3</sup> · P. Canu<sup>2</sup> · A. Glisenti<sup>1,3</sup>

Received: 29 May 2017 / Accepted: 3 October 2017  
© Springer Science+Business Media, LLC 2017

**Abstract** The reactivity of  $\text{Bi}_{0.5}\text{Sr}_{0.5}\text{MnO}_3$ ,  $\text{Bi}_{0.5}\text{Sr}_{0.5}\text{Mn}_{0.7}\text{Cu}_{0.3}\text{O}_3$ ,  $\text{Bi}_{0.5}\text{Sr}_{0.5}\text{Mn}_{0.7}\text{Ni}_{0.3}\text{O}_3$ ,  $\text{La}_{0.5}\text{Sr}_{0.5}\text{Mn}_{0.7}\text{Cu}_{0.3}\text{O}_3$  and  $\text{La}_{0.5}\text{Sr}_{0.5}\text{Mn}_{0.7}\text{Ni}_{0.3}\text{O}_3$  in ethanol steam reforming was studied. Different steam to carbon ratios have been tested (therefore referred as  $S/C = 1.5$ , and  $S/C = 6$ ). The effect of an ad hoc reduction pre-treatment

was also investigated. Ethanol conversion is highest in  $\text{La}_{0.5}\text{Sr}_{0.5}\text{Mn}_{0.7}\text{Ni}_{0.3}\text{O}_3$  and significant selectivity toward hydrogen and  $\text{CO}_2$  is observed. The reduction pre-treatment is more effective on nickel containing catalysts, enhancing both ethanol conversion and  $\text{H}_2$  and  $\text{CO}_2$  selectivity.

---

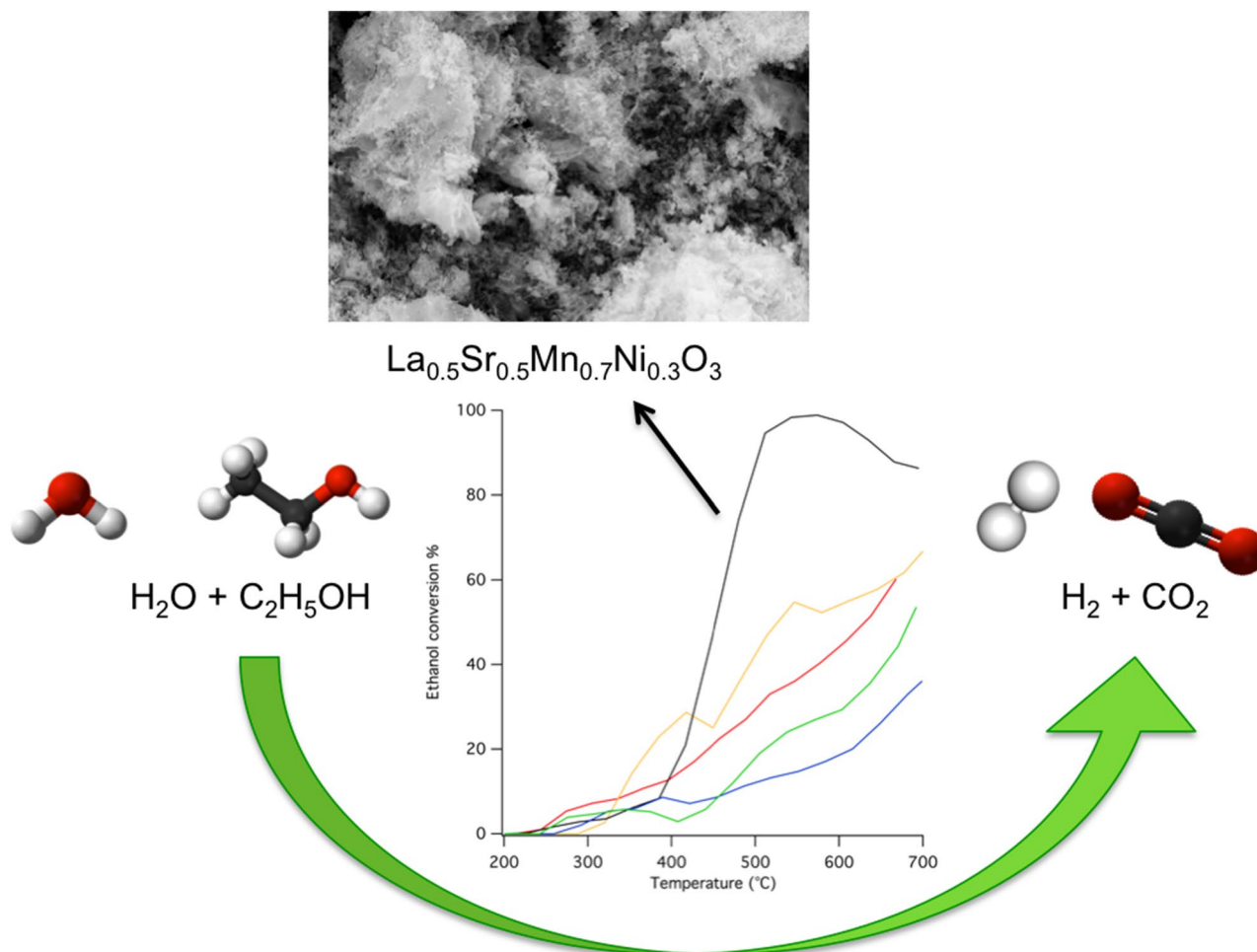
✉ G. Perin  
giovanni.perin.1@studenti.unipd.it

<sup>1</sup> Chemical Sciences Department, University of Padova, Via F. Marzolo, 1, Padova 35131, Italy

<sup>2</sup> Industrial Engineering Department, University of Padova, Via F. Marzolo, 9, Padova 35131, Italy

<sup>3</sup> CNR-ISTM, INSTM; Chemical Sciences Department, University of Padova, Via F. Marzolo, 1, 35131 Padova, Italy

## Graphical Abstract



**Keywords** Perovskites · Manganese · Steam reforming · IT-SOFC · Ethanol

## 1 Introduction

Ethanol is an interesting hydrogen vector and thus an energy vector when considering, as an example, a coupled application in fuel cells. Hydrogen can derive from ethanol steam reforming (ESR) [1, 2]; in this reaction the use of a catalyst is fundamental because both selectivity and activity depend on catalyst composition. Several catalysts have been investigated: oxide-based, metal and noble metal based. Among these, Ni-containing catalysts revealed to be interesting being active but less expensive than noble metal based ones. Ni/Al<sub>2</sub>O<sub>3</sub> converted 100% ethanol at 400 °C with 91% selectivity for H<sub>2</sub> [3]. The addition of La<sub>2</sub>O<sub>3</sub> was suggested to decrease catalyst deactivation due to carbon [4]. The use of La containing perovskites was

also investigated [5] with the aim of improving the catalytic performance, decreasing deactivation and avoiding Ni sintering, moreover many perovskites display mixed ionic and electronic conductivity, which makes them appealing for a use in solid oxide fuel cells (SOFC). In this contribution several Mn-containing perovskite-based catalysts are studied in ESR; manganese presence, in fact, was observed to reduce carbon deposition and promote catalytic activity [6, 7], to the best of our knowledge this particular type of perovskites have never been investigated before. The reactivity obtained by doping manganites with Ni or Cu was compared. Moreover, in order to test the possibility to decrease the use of Lanthanum, a Critical Raw Material, Bi based perovskites were studied. In all these catalysts part of the A-site cation (La or Bi) is substituted by Sr. The use of this element in the catalyst formulation is intended to increase the activity in redox reactions (increasing the oxygen mobility and the oxidation state of the cation in B) and acting as alkaline promoter.

## 2 Experimental

### 2.1 Catalyst Preparation

$\text{Bi}_{0.5}\text{Sr}_{0.5}\text{MnO}_3$  (BSM),  $\text{Bi}_{0.5}\text{Sr}_{0.5}\text{Mn}_{0.7}\text{Cu}_{0.3}\text{O}_3$  (BSMC),  $\text{Bi}_{0.5}\text{Sr}_{0.5}\text{Mn}_{0.7}\text{Ni}_{0.3}\text{O}_3$  (BSMN),  $\text{La}_{0.5}\text{Sr}_{0.5}\text{Mn}_{0.7}\text{Cu}_{0.3}\text{O}_3$  (LSMC) and  $\text{La}_{0.5}\text{Sr}_{0.5}\text{Mn}_{0.7}\text{Ni}_{0.3}\text{O}_3$  (LSMN) powders were synthesized by citrate route [8], starting from adequate precursors:  $\text{Bi}(\text{C}_6\text{H}_5\text{O}_7)$  (99.99% purity, Sigma-Aldrich),  $\text{Sr}(\text{NO}_3)_2$  ( $\geq 98\%$ , Sigma-Aldrich),  $\text{La}_2\text{O}_3$  (99.9%, Aldrich),  $\text{Mn}(\text{CH}_3\text{COO})_2 \cdot 4\text{H}_2\text{O}$  ( $\geq 99.0\%$ , Sigma-Aldrich),  $\text{CuO}$  (98%, Sigma-Aldrich),  $\text{Ni}(\text{NO}_3)_2 \cdot 6\text{H}_2\text{O}$  ( $\geq 97\%$ , Sigma-Aldrich). After the dissolution of the precursors, achieved with water in case of nitrates or with nitric acid ( $\geq 65\%$  Sigma-Aldrich) for oxides and bismuth citrate, citric acid monohydrate ( $\geq 99.0\%$ , Sigma-Aldrich) is added in amount of 1.9:1 with respect of the total amount of cations. Ammonia (30–33% in water, Sigma-Aldrich) is added while stirring, until pH 6.5 is reached. The solution is then concentrated by evaporation at  $90^\circ\text{C}$  until the formation of a gel that is heated for 2 h at  $400^\circ\text{C}$ . The ash-like, spongy resulting material is ground into powder and then calcined for 6 h at  $1000^\circ\text{C}$  in air atmosphere.

### 2.2 Catalyst Characterization

X-ray diffraction patterns (XRD) were collected with a Bruker D8 Advance automatic diffractometer, with  $\text{Cu K}\alpha$  wavelength ( $\lambda = 0.154 \text{ nm}$ ) at a voltage of 40 kV and a current of 40 mA.

X-ray photoelectron spectroscopy (XPS) was recorded by a Perkin Elmer PHI 5600ci Multi Technique System, using  $\text{AlK}\alpha$  radiation (1486.6 eV) working at 250 W. The spectrometer was calibrated by assuming the binding energy (BE) of the  $\text{Au } 4f_{7/2}$  line to be 84.0 eV with respect to the Fermi level. Both extended spectra (survey—187.85 eV pass energy, 0.5, 0.05 s/step) and detailed spectra (for Bi 4f, La 3d, Sr 3d, Mn 2p, Cu 2p, Ni 2p, O 1s and C 1s—23.5 eV pass energy, 0.1, 0.1 s/step) were collected. The standard deviation in the BE values of the XPS line is 0.10 eV. The atomic percentage, after a Shirley-type background subtraction [9] was evaluated by using the PHI sensitivity factors [10, 11]. The peak positions were corrected for the charging effects by considering the C 1s peak at 285.0 eV and evaluating the BE differences.

Temperature-programmed reduction (TPR) measures were collected with a Micromeritics AutoChem II 2920. Experiments were performed in a downstream fixed bed quartz tube reactor with a 5% $\text{H}_2$ /Ar stream at 50 sccm/min, raising temperature from RT to  $900^\circ\text{C}$  at  $10^\circ\text{C}/\text{min}$  speed; hydrogen consumption was monitored by a TCD detector.

BET surface specific area was measured with a Micromeritics AutoChem II 2920, after a degassing treatment (2 h at  $350^\circ\text{C}$ ).

### 2.3 Catalytic Tests

Steam reforming of ethanol was conducted in a continuous-flow fixed-bed quartz reactor at atmospheric pressure. A water–ethanol solution ( $\text{H}_2\text{O}:\text{C}_2\text{H}_5\text{OH}$  ratios of 3:1 and 12:1, having  $\text{S/C} = 1.5$  and  $\text{S/C} = 6$ , respectively) was fed by a syringe pump at  $8.3 \mu\text{l}/\text{min}$  speed, and vaporized at  $170^\circ\text{C}$  on a SiC bed, using Ar as carrier gas, (flux controlled by Brooks mass flow controller). Effluent gases were analysed by Agilent 7820 gas-chromatograph, equipped with thermal conductivity (TCD) and flame ionization (FID) detectors. Water, ethanol, acetaldehyde and  $\text{CO}_2$  were separated by the PoraPak-Q column; for hydrogen, CO and methane analysis a Molsieve ms5A column was used. The catalytic behaviour was investigated with or without an activation treatment (in 5% $\text{H}_2$ /Ar stream) specifically chosen on the basis of TPR measurements.

## 3 Results and Discussion

### 3.1 Characterization

As it is observed from XRD patterns (Fig. 1), the substitution of lanthanum with bismuth occurs without drawbacks

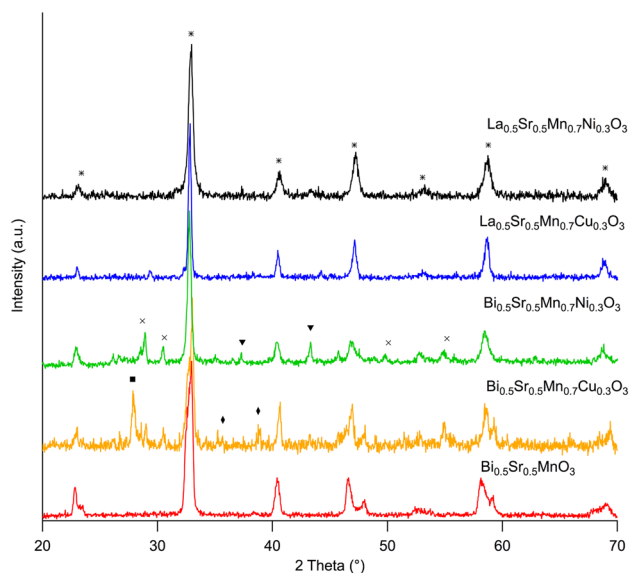


**Fig. 1** XRD patterns of  $\text{Bi}_{0.5}\text{Sr}_{0.5}\text{MnO}_3$  (red),  $\text{Bi}_{0.5}\text{Sr}_{0.5}\text{Mn}_{0.7}\text{Cu}_{0.3}\text{O}_3$  (yellow),  $\text{Bi}_{0.5}\text{Sr}_{0.5}\text{Mn}_{0.7}\text{Ni}_{0.3}\text{O}_3$  (green),  $\text{La}_{0.5}\text{Sr}_{0.5}\text{Mn}_{0.7}\text{Cu}_{0.3}\text{O}_3$  (blue) and  $\text{La}_{0.5}\text{Sr}_{0.5}\text{Mn}_{0.7}\text{Ni}_{0.3}\text{O}_3$  (black) powders. Symbols stand for: asterisk (perovskite); filled rhombus (CuO); filled inverted triangle (NiO); cross ( $\text{Bi}_2\text{O}_3$ ); filled square ( $\text{Bi}_2\text{Mn}_4\text{O}_{10}$ )

in the crystalline structure of BSM. In the B-site doped compounds, beside the major perovskitic crystalline phase, traces of oxides segregation ( $\text{CuO}$ ,  $\text{NiO}$ ,  $\text{Bi}_2\text{O}_3$ , and  $\text{Bi}_2\text{Mn}_4\text{O}_{10}$ ) can be seen. The calculated values for t-factor ( $\text{BSM} = 0.9838$ ;  $\text{BSMC} = 0.9660$ ;  $\text{BSMN} = 0.9719$ ;  $\text{LSMC} = 0.9742$ ;  $\text{LSMN} = 0.9801$ ) suggest the possibility that B-doping can contribute to the instability of the crystalline structure.

The following surface area values were obtained for  $\text{Bi}_{0.5}\text{Sr}_{0.5}\text{MnO}_3$  ( $13 \text{ m}^2/\text{g}$ ),  $\text{Bi}_{0.5}\text{Sr}_{0.5}\text{Mn}_{0.7}\text{Cu}_{0.3}\text{O}_3$  ( $10 \text{ m}^2/\text{g}$ ),  $\text{Bi}_{0.5}\text{Sr}_{0.5}\text{Mn}_{0.7}\text{Ni}_{0.3}\text{O}_3$  ( $10 \text{ m}^2/\text{g}$ ),  $\text{La}_{0.5}\text{Sr}_{0.5}\text{Mn}_{0.7}\text{Cu}_{0.3}\text{O}_3$  ( $10 \text{ m}^2/\text{g}$ ) and  $\text{La}_{0.5}\text{Sr}_{0.5}\text{Mn}_{0.7}\text{Ni}_{0.3}\text{O}_3$  ( $24 \text{ m}^2/\text{g}$ ).

O 1s XPS peaks (Fig. 2), show two contributions due to perovskitic oxygen ( $529.5 \text{ eV}$ ), and to the presence of carbonates and hydroxides ( $531.2\text{--}531.7 \text{ eV}$ ) [8, 12–15]. It is worth to notice that nickel doping seems to induce lower hydroxyls and carbonates formation with respect to copper. The position of Sr 3d peaks ( $132.5$  and  $133.8 \text{ eV}$  for  $3d_{5/2}$ ,  $3d_{3/2}$ ) is consistent with the presence of perovskite and carbonate species. Mn $2p_{3/2}$  and Mn $2p_{1/2}$  binding energies ( $642.1$  and  $653.5 \text{ eV}$ , respectively), confirm the presence, in all the samples, of both Mn(III) and Mn(IV), whose oxides are reported in literature at  $641.7$  and  $642.2 \text{ eV}$ , respectively [12, 13].

Cu $2p_{3/2}$  signal at  $934.0 \text{ eV}$ , marks the presence of hydroxylated copper and shake-up peaks characteristic of Cu(II) [14, 15]. Ni $2p_{3/2}$  peak ( $954.4 \text{ eV}$ ) is consistent with the presence of Ni(II) in the outmost layers, as confirmed by the shake-up peaks (at  $862.0$  and  $881.0 \text{ eV}$ ). The position and shape of bismuth ( $159.0 \text{ eV}$ ), and lanthanum ( $834.2 \text{ eV}$ ) are consistent with the presence of these elements in the expected oxidation state [14].

XPS quantitative analysis (Table 1) shows a surface segregation of bismuth for BSMC and BSMN, reducing the surface amount of B-site dopants; BSM and BSMN also suffer from Sr surface segregation. On the contrary, lanthanum based materials seem not to be affected by segregation phenomena in the same extent, displaying a nearly stoichiometric composition of the surface. LSMC, in contrast with BSMC, presents a high surface content of copper, with a B/A cations ratio of 0.99. A similar trend is observable for nickel in LSMN, in which B/A is higher than one.

The TPR profile (Fig. 3) of BSM reveals a peak at  $586 \text{ }^\circ\text{C}$  and weak contributions at about  $400$ ,  $730$ , and  $825 \text{ }^\circ\text{C}$ . The signal at  $586 \text{ }^\circ\text{C}$  is attributed to the reduction Bi(III) to Bi(0) and Mn(IV) to Mn(III) [16]. The weak signals at  $400$ ,  $730$  and  $825 \text{ }^\circ\text{C}$  can be due to weakly adsorbed oxygen and to the two step reduction of Mn(III) to Mn(II) respectively, which was previously reported to proceed by means of  $\text{Mn}_3\text{O}_4$  formation [17, 18]. The addition of Cu causes a slight shift of the Bi(III) and Mn(IV) reduction peak toward higher temperature ( $679 \text{ }^\circ\text{C}$ ), this may be

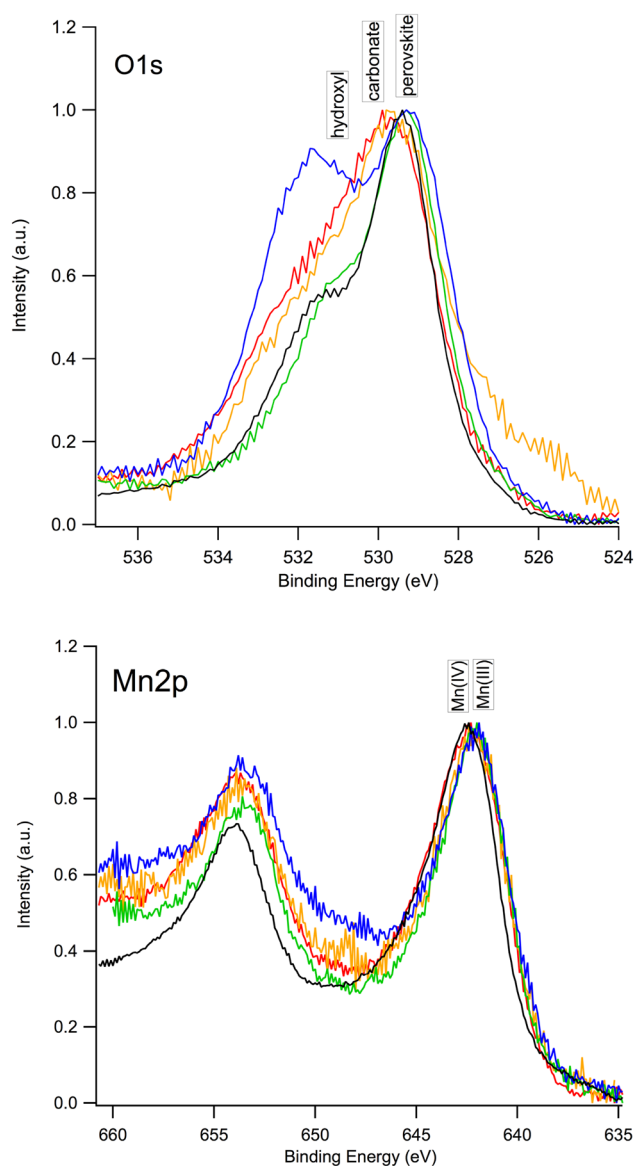


**Fig. 2** XPS spectra of O 1s and Mn 2p peaks for  $\text{Bi}_{0.5}\text{Sr}_{0.5}\text{MnO}_3$  (red),  $\text{Bi}_{0.5}\text{Sr}_{0.5}\text{Mn}_{0.7}\text{Cu}_{0.3}\text{O}_3$  (yellow),  $\text{Bi}_{0.5}\text{Sr}_{0.5}\text{Mn}_{0.7}\text{Ni}_{0.3}\text{O}_3$  (green),  $\text{La}_{0.5}\text{Sr}_{0.5}\text{Mn}_{0.7}\text{Cu}_{0.3}\text{O}_3$  (blue) and  $\text{La}_{0.5}\text{Sr}_{0.5}\text{Mn}_{0.7}\text{Ni}_{0.3}\text{O}_3$  (black)

due to the severe surface segregation of Bi; the reduction of Cu(II) is observed at  $447 \text{ }^\circ\text{C}$ . The substitution with Ni induces a shift of the Bi(III) and Mn(IV) peak to lower temperature ( $497 \text{ }^\circ\text{C}$ ). Nonetheless, it is possible to observe that the substitution with copper or nickel in the B-site shifts the onset of reduction to lower temperatures, as was already observed on systems of the type  $\text{LaB}_{0.2}\text{Mn}_{0.8}\text{O}_3$  [19]. In La containing perovskites, the temperature of the reduction is lower, this is particularly evident in LSMN sample, which shows two intense reduction peaks at  $350$  and  $450 \text{ }^\circ\text{C}$ .

**Table 1** Surface composition of  $\text{Bi}_{0.5}\text{Sr}_{0.5}\text{MnO}_3$ ,  $\text{Bi}_{0.5}\text{Sr}_{0.5}\text{Mn}_{0.7}\text{Cu}_{0.3}\text{O}_3$ ,  $\text{Bi}_{0.5}\text{Sr}_{0.5}\text{Mn}_{0.7}\text{Ni}_{0.3}\text{O}_3$ ,  $\text{La}_{0.5}\text{Sr}_{0.5}\text{Mn}_{0.7}\text{Cu}_{0.3}\text{O}_3$  and  $\text{La}_{0.5}\text{Sr}_{0.5}\text{Mn}_{0.7}\text{Ni}_{0.3}\text{O}_3$ 

$\text{Bi}_{0.5}\text{Sr}_{0.5}\text{MnO}_3$	Bi	Sr	Mn	
Experimental	25.3	31.7	43.0	
Nominal	25	25	50	
$\text{Bi}_{0.5}\text{Sr}_{0.5}\text{Mn}_{0.7}\text{Cu}_{0.3}\text{O}_3$	Bi	Sr	Mn	Cu
Experimental	49.6	21.7	24.3	4.4
Nominal	25	25	35	15
$\text{Bi}_{0.5}\text{Sr}_{0.5}\text{Mn}_{0.7}\text{Ni}_{0.3}\text{O}_3$	Bi	Sr	Mn	Ni
Experimental	37.4	31.6	25.8	5.2
Nominal	25	25	35	15
$\text{La}_{0.5}\text{Sr}_{0.5}\text{Mn}_{0.7}\text{Cu}_{0.3}\text{O}_3$	La	Sr	Mn	Cu
Experimental	17.7	33.5	29.0	19.8
Nominal	25	25	35	15
$\text{La}_{0.5}\text{Sr}_{0.5}\text{Mn}_{0.7}\text{Ni}_{0.3}\text{O}_3$	La	Sr	Mn	Ni
Experimental	22.6	23.2	42.1	12.1
Nominal	25	25	35	15

Nominal composition values are determined by the stoichiometric amounts

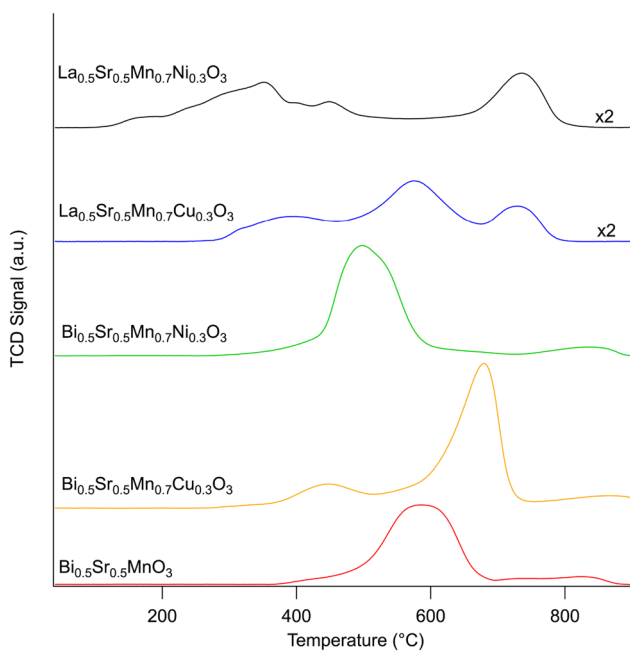


**Fig. 3** TPR profiles of  $\text{Bi}_{0.5}\text{Sr}_{0.5}\text{MnO}_3$  (red),  $\text{Bi}_{0.5}\text{Sr}_{0.5}\text{Mn}_{0.7}\text{Cu}_{0.3}\text{O}_3$  (yellow),  $\text{Bi}_{0.5}\text{Sr}_{0.5}\text{Mn}_{0.7}\text{Ni}_{0.3}\text{O}_3$  (green),  $\text{La}_{0.5}\text{Sr}_{0.5}\text{Mn}_{0.7}\text{Cu}_{0.3}\text{O}_3$  (blue) and  $\text{La}_{0.5}\text{Sr}_{0.5}\text{Mn}_{0.7}\text{Ni}_{0.3}\text{O}_3$  (black)

In all samples, the comparison between the estimated and experimental  $\text{H}_2$  consumptions (Cu and Ni were considered divalent) reveals the complete reduction of Bi(III) to Bi(0) and of Mn(IV) to Mn(III), suggesting that Mn(III) to Mn

(II) reduction may be more difficult in samples which have a higher crystallinity degree [18].

### 3.2 Catalytic Activity

ESR catalytic test results obtained at  $S/C = 1.5$  (Fig. 4a), indicate that ethanol conversion reaches 100% at 600 °C (80% at 470 °C) with  $\text{La}_{0.5}\text{Sr}_{0.5}\text{Mn}_{0.7}\text{Ni}_{0.3}\text{O}_3$ .

Lanthanum replacement with bismuth reduces ethanol conversion from 90 to 43% (at 700 °C) in nickel doped samples, suggesting a cooperative effect between La and Ni; this effect is less evident when doping with copper. Both BSMC and LSMC reach about 30% ethanol conversion at 700 °C; BSM reaches 50% conversion at 700 °C. The XPS compositions suggest that the presence on the surface of significant amounts of Mn and Ni can be fundamental in order to obtain high conversions (the atomic % of these elements is maximum in LSMN). As for the other B-site doped materials, the surface segregation of Bi (in BSMC) and of Sr (in LSMC) can significantly reduce the catalyst activity, this effect pronounced even in the case of BSMN. A lower amount of nickel (which is active in C–C cleavage) could enhance the production  $\text{C}_2$  by-products (e.g. ethylene) and thus of undesired carbon, leading to catalyst deactivation.

The main products detected are hydrogen and acetaldehyde (Table 2) in all cases but LSMN. For this catalyst the main products are hydrogen,  $\text{CO}_2$  and  $\text{CH}_4$ ; acetaldehyde is also observed, but only in the temperature range from 400 to 600 °C. Bismuth-based materials seem to favor dehydration

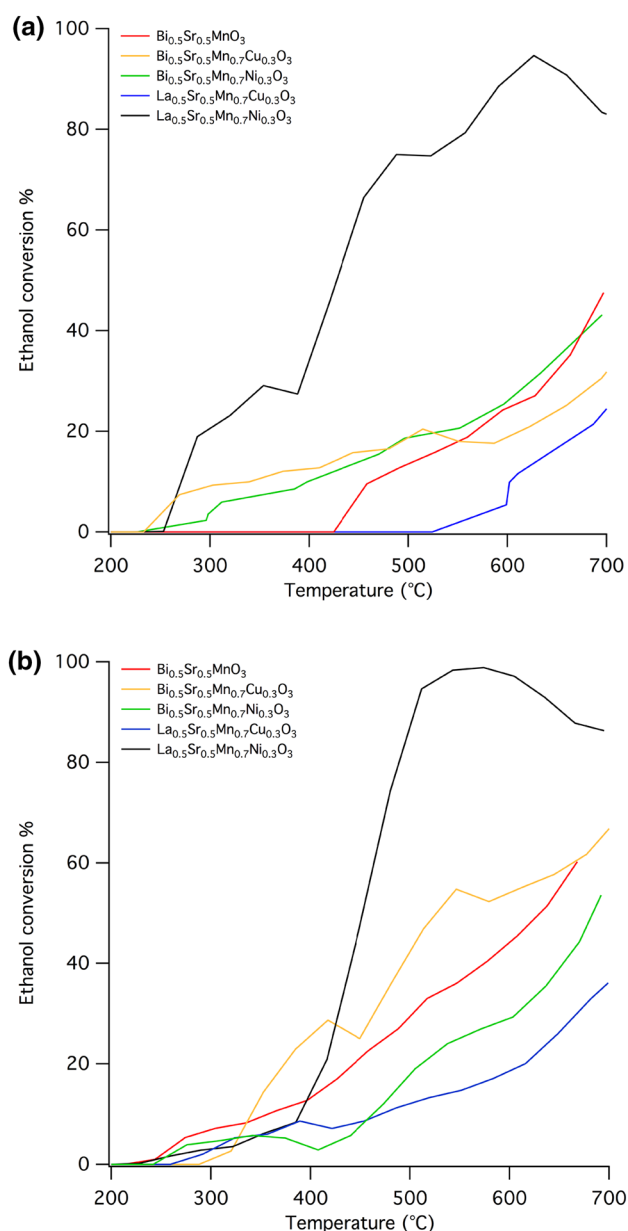


**Fig. 4** Ethanol conversion (as function of temperature) of  $\text{Bi}_{0.5}\text{Sr}_{0.5}\text{MnO}_3$  (red),  $\text{Bi}_{0.5}\text{Sr}_{0.5}\text{Mn}_{0.7}\text{Cu}_{0.3}\text{O}_3$  (yellow),  $\text{Bi}_{0.5}\text{Sr}_{0.5}\text{Mn}_{0.7}\text{Ni}_{0.3}\text{O}_3$  (green),  $\text{La}_{0.5}\text{Sr}_{0.5}\text{Mn}_{0.7}\text{Cu}_{0.3}\text{O}_3$  (blue) and  $\text{La}_{0.5}\text{Sr}_{0.5}\text{Mn}_{0.7}\text{Ni}_{0.3}\text{O}_3$  (black) at different steam to carbon ratios:  $\text{S/C} = 1.5$  (a) and  $\text{S/C} = 6$  (b)

route instead of dehydrogenation, in particular in the case of BSMC.

Reactivity was further investigated with steam to carbon ratio of 6 (Fig. 4b). The higher amount of water produces higher conversions for ethanol: for LSMN almost complete conversion is observed at 500 °C; for the other catalysts at 700 °C the ethanol conversion ranges from 35% (LSMC) to 54% (BSMN), to 60% (BSM), to 65% (BSMC). As in the former case, the main products detected are hydrogen

**Table 2** Ethanol conversion values,  $\text{H}_2$ ,  $\text{CO}_2$ , and acetaldehyde yields values obtained at 700 °C for the different catalysts in the ethanol steam reforming reaction; the conversions and yields obtained at 600 °C are also reported for  $\text{La}_{0.5}\text{Sr}_{0.5}\text{Mn}_{0.7}\text{Ni}_{0.3}\text{O}_3$ ; this, in fact, is the temperature at which the catalyst performance are maxima

Catalyst	X EtOH	Y $\text{H}_2$	Y $\text{CO}_2$	Y $\text{CH}_3\text{CHO}$
<b>BSM</b>				
S/C = 1.5	48	7	3	32
S/C = 6	60	12	3	42
Pretreated	55	17	0	39
<b>BSMN</b>				
S/C = 1.5	43	9	3	27
S/C = 6	54	12	0	32
Pretreated	79	28	12	57
<b>BSMC</b>				
S/C = 1.5	31	10	0	17
S/C = 6	67	17	0	42
Pretreated	53	10	0	42
<b>LSMN</b>				
S/C = 1.5	95	61	32	9.5
S/C = 6	100	62 (85)	45 (80)	10 (0)
Pretreated	96 (100)	66 (90)	10 (20)	31 (0)
<b>LSMC</b>				
S/C = 1.5	25	3	0	18
S/C = 6	36	5	0	22
Pretreated	39	8	0	33

and acetaldehyde for all catalysts but LSMN, for which  $\text{H}_2$  and  $\text{CO}_2$  are the main products;  $\text{CH}_4$  and acetaldehyde are observed only at temperatures higher than 600 °C.

A pre-treatment of reduction (5%  $\text{H}_2/\text{Ar}$ ), chosen on the basis of TPR measurement, was carried out in order to investigate the effect of activation on activity and selectivity. The reduction was carried out with the aim of enhancing the surface content of active B-site reduced cations, (particularly in of BSMC and BSMN, whose content in copper and nickel was very low) with a mild treatment, to avoid the complete reduction of perovskite.

The reduction temperature was thus chosen *ad hoc* for each catalyst, considering the first reduction process of Bi(III) and Mn(IV) as the main criteria. The chosen values are:  $\text{Bi}_{0.5}\text{Sr}_{0.5}\text{MnO}_3$  (560 °C),  $\text{Bi}_{0.5}\text{Sr}_{0.5}\text{Mn}_{0.7}\text{Cu}_{0.3}\text{O}_3$  (525 °C),  $\text{Bi}_{0.5}\text{Sr}_{0.5}\text{Mn}_{0.7}\text{Ni}_{0.3}\text{O}_3$  (470 °C),  $\text{La}_{0.5}\text{Sr}_{0.5}\text{Mn}_{0.7}\text{Cu}_{0.3}\text{O}_3$  (450 °C) and  $\text{La}_{0.5}\text{Sr}_{0.5}\text{Mn}_{0.7}\text{Ni}_{0.3}\text{O}_3$  (400). XPS was performed soon after reduction, to evaluate the presence of differences in surface composition with fresh samples. The comparison between the atomic percentages before and after reduction revealed an enrichment of B-site cations (reported to be responsible of catalytic activity), this phenomenon is more relevant in the case of BSMN (Table 3).

**Table 3** Surface composition of  $\text{Bi}_{0.5}\text{Sr}_{0.5}\text{Mn}_{0.7}\text{Cu}_{0.3}\text{O}_3$  and  $\text{Bi}_{0.5}\text{Sr}_{0.5}\text{Mn}_{0.7}\text{Ni}_{0.3}\text{O}_3$  after the reduction ( $5\%\text{H}_2/\text{Ar}$ ) treatment

BSMC	Bi	Sr	Mn	Cu
Reduced	44.7	20.0	23.3	12.0
Fresh	49.6	21.7	24.3	4.4
Nominal	25	25	35	15
BSMN	Bi	Sr	Mn	Ni
Reduced	23.3	28.6	42.7	5.3
Fresh	37.4	31.6	25.8	5.2
Nominal	25	25	35	15

Surface cation compositions of fresh catalysts and nominal values are reported for comparison

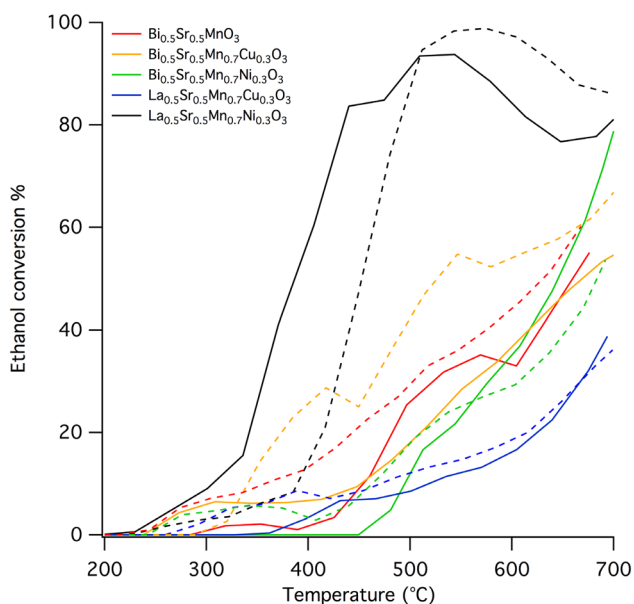


**Fig. 5** Ethanol conversion (as function of temperature) of pre-reduced  $\text{Bi}_{0.5}\text{Sr}_{0.5}\text{MnO}_3$  (red),  $\text{Bi}_{0.5}\text{Sr}_{0.5}\text{Mn}_{0.7}\text{Cu}_{0.3}\text{O}_3$  (yellow),  $\text{Bi}_{0.5}\text{Sr}_{0.5}\text{Mn}_{0.7}\text{Ni}_{0.3}\text{O}_3$  (green),  $\text{La}_{0.5}\text{Sr}_{0.5}\text{Mn}_{0.7}\text{Cu}_{0.3}\text{O}_3$  (blue) and  $\text{La}_{0.5}\text{Sr}_{0.5}\text{Mn}_{0.7}\text{Ni}_{0.3}\text{O}_3$  (black) tested under  $S/C=6$ . Ethanol conversion of unreduced samples tested in same conditions is reported in dashed lines for comparison

Steam reforming tests were carried out on the activated catalysts (Fig. 5) with steam to carbon ratio of 6, showing that the reduction treatment was effective on BSMN (conversion raises from 54 to 79% at 700 °C); the  $\text{CH}_4$  and  $\text{CO}_2$  yields also increase, the main products detected are still acetaldehyde and hydrogen.

These results allow thinking that an activation treatment in hydrogen can enhance catalyst performances by modifying the surface composition.

## 4 Conclusions

In this contribution several Mn based perovskites have been developed and their properties and reactivity in ESR have been tested; moreover the role of A-site cation was investigated in order to understand if La replacement with Bi represents a feasible possibility.

XRD and XPS measurements revealed the tendency to segregation of bismuth, which is more evident in B-substituted samples. Lanthanum containing catalysts seem not to be affected by segregation in the same extent; moreover, La presence seems to favor the dehydrogenation reaction path, yielding to higher  $\text{H}_2$  and  $\text{CO}_2$  production, especially in the case of LSMN. These data suggest a strong correlation between the chosen A-site cation and reaction pathway, showing the relevant role played by lanthanum in co-presence with nickel.

Beside the segregation effects, we have demonstrated that a mild reduction pretreatment, accurately chosen on the base of TPR results, could represent a solution to enrich the surface content of B-site cations and enhance the production of  $\text{H}_2$  and  $\text{CO}_2$ , as observed in particular for BSMN. This suggests the possible use of bismuth for a partial replacement of lanthanum, if paying attention to surface segregation effects. LSMN promising catalytic performances (allowing to reach 100% ethanol conversion at 500 °C with high selectivity towards  $\text{H}_2$  and  $\text{CO}_2$ ) shed light onto the possibility of using Mn-based perovskites to perform in-situ ethanol reforming in a SOFC anode. Further measurements of stability and electrochemical activity have to be performed for a deeper characterization of the material in a SOFC reaction environment.

**Acknowledgements** We gratefully thank Cariparo, the European Union's 7th Framework Programme under Grant Agreement No. 280890- NEXT-GEN-CAT and European Union's Horizon 2020 research and innovation programme under Grant Agreement No. 686086 PARTIAL-PGM for partial financing. The funding was provided by Fondazione Cassa di Risparmio di Padova e Rovigo.

## References

1. Haryanto A, Pernando S, Murali N, Adhikari S (2005) *Energy Fuels* 19:2098–2106
2. Ni M, Leung DYC, Leung MKH (2007) *Int J Hydrog Energy* 32:3238–3247
3. Mattos LV, Jacobs G, Davis BH, Noronha FB (2012) *Chem Rev* 112:4094–4123
4. Liu H, Wierzbicki D, Debeka R, Motak M, Grzybek T, Da P, Costa ME, Gálvez (2016) *Fuel* 182:8–16
5. Chena H, Yua H, Penga F, Yanga G, Wanga H, Yanga J, Y. Tang (2010) *Chem Eng J* 160:333–339
6. Koike M, Ishikawa C, Li D, Wangb L, Nakagawab Y, Tomishige K (2013) *Fuel* 103:122–129
7. Huang L, Zhanga F, Chenb R, Hsu AT (2012) *Int J Hydrog Energy* 37:15908–15913 (**15909 less**)
8. Natile MM, Poletto F, Galenda A, Glisenti A, Montini T, De Rogatis L, Fornasiero P (2008) *Chem Mater* 20:2314
9. Shirley DA (1972) *Phys Rev B* 5:4709–4714
10. Moulder JF, Stickle WF, Sobol PE, Bomben KD (1992) In: Chastain J (ed) *Handbook of X-ray photoelectron spectroscopy*. Physical Electronics, Eden Prairie
11. Briggs D, Riviere JC (1983) In: Briggs D, Seah MP (eds) *Practical surface analysis*. Wiley, New York
12. Glisenti A, Natile MM, Galenda A (2009) *Surf Sci Spectra* 16:64–74
13. Glisenti A, Galenda A, Natile MM (2009) *Surf Sci Spectra* 16:83–94
14. NIST XPS Database 20, Version 4.1 (Web Version)
15. Glisenti A, Pacella M, Guiotto M, Natile MM, Canu P; (2016) *Appl Catal B* 180:4–105
16. Ivanova AS, Slavinskaya EM, Mokrinskii VV, Polukhina IA, Tsybulya SV, Prosvirin IP, Bukhtiyarov VI, Rogov VA, Zaikovskii VI, Noskov AS (2004) *J Catal* 221:213–224
17. Buciuman F, Patcas F, Zsakó J (2000) *J Therm Anal Calorim* 61:819–825
18. Stobbe ER, de Boer BA, Geus JW (1999) *Catal Today* 47:161–167
19. Zhang C, Wang C, Zhan W, Guo Y, Guo G, Lu A, Baylet A, Giroir-Fendler A (2013) *Appl Catal B* 129:509–516